VNU Journal of Science: Mathematics - Physics

Journal homepage: https://js.vnu.edu.vn/MaP

Original Article

Numerical Investigation of Optical Properties in Carbon Tetrachloride-Filled Photonic Crystal Fibers

Nguyen Thi Thuy*, Nguyen Thi Oanh

University of Education, Hue University, 34 Le Loi, Hue City, Vietnam

Received 11 May 2023
Revised 13 June 2023; Accepted 16 June 2023

Abstract: In this work, we design circular lattice photonic crystal fibers using Lumerical Mode Solution software, its hollow core filled with carbon tetrachloride. Optical properties including effective refractive index, chromatic dispersion, nonlinearity, and fiber loss were investigated numerically in detail based on solving Maxwell's wave equations. The small effective mode areas of only a few μm^2, and confinement loss as low as 14.799 dB/m at specific pump wavelengths were obtained. It was found that near-zero ultra-flattened chromatic dispersion with fluctuations of ±0.44 ps/nm.km spans from 1300 to 1830 nm. Three photonic crystal fibers with optimal structure and features were suggested for broadband supercontinuum generation orientation.

Keywords: Photonic crystal fibers, carbon tetrachloride, ultra-flattened dispersion, small effective area, low confinement loss.

1. Introduction

In recent years, silica-based liquid-core photonic crystal fibers (LPCFs) are becoming one of the highly nonlinear mediums, which greatly improve the supercontinuum generation (SC) efficiency because the traditional glass core fibers have revealed limitations in terms of transmission range for SC spectral extension. Given the flexibility in structural design, some LPCFs use highly nonlinear liquids such as toluene [1-4], chloroform [5-7], benzene [8, 9], nitrobenzene [10-14], carbon disulfide [15], tetrachlorethylene [16]. Although the LPCFs mentioned above show more advantages in terms of improving the dispersion for a more extended SC spectrum than the solid core PCFs, other non-linear characteristic quantities have not yet reached the desired value. This partially limits the quality of the

* Corresponding author.
E-mail address: ntoanh915@gmail.com

https//doi.org/10.25073/2588-1124/vnumap.4850

SC generation. Two optimal LPCFs (with toluene) were reported in [4] with relatively low dispersion values below 7.9 ps/nm.km and high nonlinear coefficients around several thousand $W^{-1}.km^{-1}$ at 1.55 μm pump wavelength, but a relatively large effective mode area was also found. The LPCF with chloroform [5] exposed a flat dispersion but a rather high dispersion value of −24 ps/nm.km at 1.03 μm, the effective mode area having a smaller value of 4.5 μm^2 was also shown in this publication. Dispersion values were as high as 33.7 ps/nm.km at 1.03 μm was shown in [10] with nitrobenzene-LPCF but the SC spectrum was significantly extended due to the relatively high nonlinear coefficient. A large effective mode area of 16.67 μm^2 and 359.1 μm^2, respectively with pumping wavelengths of 1.56 μm and 1.03 μm for the two proposed tetrachlorethylene-infiltrated fibers has been shown in [16]. In this case, the nonlinear coefficient is also not as high as expected, but the dispersion value is flat and quite small at 3.20 ps/nm.km and -4.85 ps/nm.km, respectively. Some common characteristics can be seen when studying SC generation using these LPCFs: The chromatic dispersion profiles including flatness and relatively low values at the respective pump wavelengths, were markedly improved. Research groups have obtained a number of characteristic quantities with preferred values such as effective mode area, nonlinear coefficient, confinement loss or fiber attenuation. It is not difficult to control the all-normal and anomalous dispersion based on the optimization of the design structure. The zero dispersion wavelengths (ZDWs) tend to shift towards long wavelength regions which favors the choice of pump wavelength. The SC spectrum is broadened thanks to the main nonlinear effects including soliton dynamics (soliton fission (SF), soliton self-frequency shift (SSFS), stimulated Raman scattering, etc.) when the fiber is excited in the anomalous dispersion regime. In the case of fibers pumped in an all-normal dispersion region, self-phase modulation (SPM), optical wave breaking (OWB), and four-wave mixing (FWM) are responsible for spectral expansion [17].

LPCFs with carbon tetrachloride have demonstrated the ability to broaden the SC spectrum by numerical simulation [18-20] and experimentally [21-23]. Carbon tetrachloride has a nonlinear coefficient ($n_2 = 1.53\times10^{-19}$ m^2/W) at λ = 1.064 μm [23] which is about 5 times higher than that of silica ($n_2 = 2.74\times10^{-20}$ m^2/W), is a favorable factor to improve chromatic dispersion properties and increase the quality of SC spectrum. LPCFs with carbon tetrachloride will be more convenient to fabricate fibers in practice because of their lower toxicity when compared to carbon disulfide, nitrobenzene, benzene, or toluene [24, 25] despite the smaller nonlinear coefficient. The coupling between liquid core fibers and typical silica fibers will be highly efficient thank the similarity between the linear refractive indices of carbon tetrachloride and fused silica [26, 27]. The above interesting characteristics have made carbon tetrachloride selected to fill the hollow core of the fibers with the desire to optimize the characteristic quantities. In the study [18], LPCFs were designed with a regular hexagonal lattice, the distance between two adjacent air holes (lattice constant Λ) and the diameter of the air holes (d) did not differ. Two optimal fibers with anomalous and all-normal dispersion were obtained, dispersion values of 12 ps/nm.km and − 4.37 ps/nm.km at wavelengths of 1.35 μm and 1.55 μm respectively. The attenuation had a rather low value at 1.4 μm of 0.0185 dB/m and 0.0158 dB/m. These two fibers were confirmed to produce an octave-spanning broad spectrum with high coherence using an input pulse of 300 fs with 0.8 nJ. By making a difference in the air hole diameters of the first ring and other rings in the cladding of LPCFs, the papers [19, 20] also demonstrated the ability to improve the flatness and the value of the dispersion. This results in a broad, flat-top SC spectrum with low input power when using these LPCFs with a circular and square lattice. With the same pump wavelength of 1.3 μm, low anomalous dispersion was achieved of 1.015 ps/nm.km with circular lattice fibers [19] and 1.331 ps/nm.km with square lattice fibers [20]. Meanwhile, dispersion value as well as other characteristic quantities of the experimentally investigated LPCFs in [21-23] were higher. With a larger air holes size in the first ring than the others, LPCFs [21] were fabricated with a hexagonal lattice provide dispersion ranging from –280 ps/nm.km to

–15 ps/nm.km in a wavelength range of 1.0–2.5 μm, the flatness was markedly improved compared with carbon tetrachloride-unfilled PCFs.

In this work, we distinguish between the distance from the core center to the air holes in the first ring (Λ_1) and the distance between two adjacent air holes (Λ) of carbon tetrachloride-filled fibers. Furthermore, the size of the first ring in the cladding is smaller than the others. This gives great benefits in optimizing the optical properties of the fibers. The dispersion flatness is effectively controlled, the dispersion curve is asymptotically close to the horizontal axis over the wavelength range of 530 nm, with an oscillation of ±0.44 ps/nm.km. We select three fibers with reasonable dispersion to investigate the nonlinear properties in detail. The results reveal that the characteristic quantities have suitable values to guide SC applications. The effective mode area of these fibers is 3.022 μm^2, 2.18 μm^2, and 3.58 μm^2 at the pump wavelengths 1.33 μm, 1.064 μm, and 1.55 μm, respectively. Interestingly, the dispersion values at these pump wavelengths are very low, 1.405 ps/nm.km, 3.328 ps/nm.km, and −1.938 ps/nm.km, which leads to the expectation for a broadband SC. These proposed fibers can be a new laser source for SC generation applications in the fields of biomedical sensing, temperature sensing, optical communication, etc.

2. Numerical Modeling of the PCFs

The lattice structure of the LPCFs was modeled using the commercial software Lumerical Mode Solution. The circular lattice was selected from the system's lattice types database. We choose the circular lattices PCF structure because it has high symmetry which helps to confine light tightly to the core. This contributes to improve dispersion, increases nonlinearity, and hence the SC generation efficiency i.e. better bandwidth enhancement compared to other lattices [1, 2, 20]. The fused silica and carbon tetrachloride substrates were established by declaring the refractive index coefficients from equation (1-2) (Sellmeier's equation [28] and Cauchy's equation [29]). The air holes are arranged in eight rings parallel to the axis of the hollow core. The idea of designing LPCFs with different air holes' diameters is based on reports [19-21, 30, 31]. It is not difficult to control dispersion in terms of flatness, slope, and shift of ZDWs. Even fiber loss is strongly influenced by the size of these air-hole rings. The cross-sections of the LPCFs are illustrated as shown in Fig. 1a, the core center distance to the first ring air hole is $\Lambda_1 = 1.093\Lambda$; where Λ is the center-to-center spacing between the nearest air holes. The first ring air hole diameter is set up: $d_1 = (0.3 \div 0.65)\Lambda$ with 0.05 steps, while the air hole's diameter from the second to eighth ring is constant and equal to $d_2 = 0.8\Lambda$ (Λ = 0.9 μm, 1.0 μm, 1.5 μm, 2.0 μm). The hollow core has the size calculated by the formula: $D_c = 2\Lambda - 1.2d_1$, (where D_c is the core's diameter), filled with carbon tetrachloride. The agreement between simulation theory and experiment is appreciated because it increases the possibility of actual fiber fabrication, so LPCFs should not have too small cores. In contrast, the light modes are better confined in cores that are not too large in size. Therefore, the core size must ensure these conditions. We avoid designing differently shaped air holes for fear of manufacturing complexity. In this work, the air holes are all circular, so the LPCFs could be fabricated by the performing drilling method or the stack and draw method. In the experiment, the liquid is introduced into the core by heat pumps [21]. The optical properties of the LPCF are studied in detail by numerically solving Maxwell's wave equations, with boundary conditions consisting of perfectly matched layers that minimize light leakage from the core. There are many methods to solve wave equations, but we choose the full vector finite difference eigencoding (FDE) method, which divides the cross-section of the LPCF into hundreds of thousands of rectangles of very small size (Yee's mesh) to compute propagation constants with high accuracy [32]. On each Yee mesh, the optical properties are virtually unchanged. We assume that carbon tetrachloride has no significant loss because this does not

affect the dispersion properties [18]. Fig. 1b verifies that the light after propagating is well confined within the cores of the fibers.

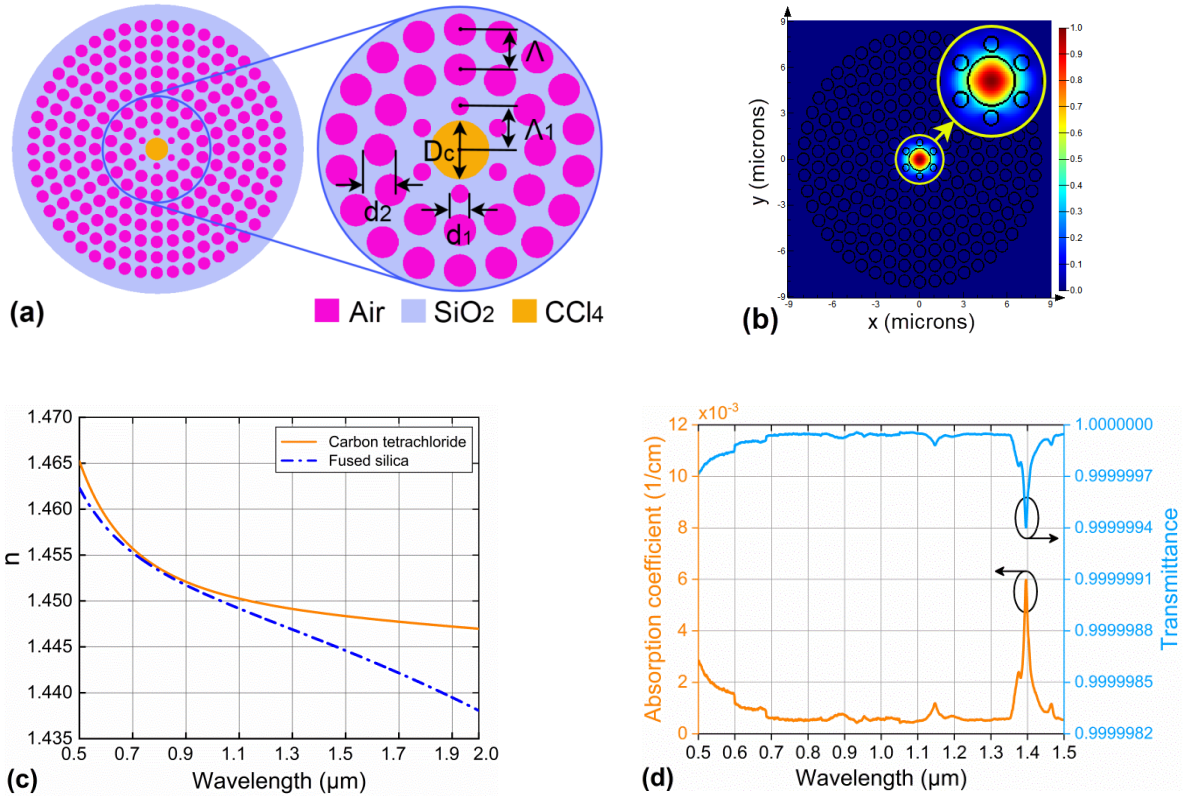

Figure 1. a) Schematic of the modeled LPCF structure with eight parallel air hole rings arranged in a circular shape, hollow core filled with carbon tetrachloride (a); Simulation of light confinement in the core of the LPCF with Λ = 1.0 μm, d_1/Λ = 0.45 (b); The dependence of the refractive index's real parts of carbon tetrachloride and fused silica on the wavelength according to the Sellmeier's and Cauchy's equation (c); The transmission and absorption spectra of carbon tetrachloride for the temperature of 20 °C with wavelengths of 0.5−1.5 μm [33].

$$n^2_{\text{fused silica}}(\lambda) = 1 + \frac{0.6961663\lambda^2}{\lambda^2 - (0.0684043)^2} + \frac{0.4079426\lambda^2}{\lambda^2 - (0.1162414)^2} + \frac{0.8974794\lambda^2}{\lambda^2 - (9.896161)^2} \quad (1)$$

$$n^2_{\text{carbon tetrachloride}}(\lambda) = 2.085608282 + 0.00053373\lambda^2 + \frac{0.012201206}{\lambda^2} + \frac{0.000056451}{\lambda^4} + \frac{0.000048106}{\lambda^6} \quad (2)$$

The effective refractive index's real part ($Re[n_{\text{eff}}]$) of carbon tetrachloride and fused silica are exposed in Fig. 1c. The difference between the two materials is quite small mainly due to the similarity in the linear refractive index of the two substances. Carbon tetrachloride is transparent over a wide wavelength range, some small absorption peaks in the 0.5−1.5 μm wavelength region are observed. The absorption peak is strongest at 1.396 μm, with a value of the imaginary part of the effective refractive index of 6.68×10^{-8}, corresponding to a fiber attenuation of 2.6 dB/m. Therefore, during the simulation

of fiber properties in the long wavelength region (greater than 1.396 μm), the fiber loss is assumed to have a similar value [33].

3. Simulation Results and Analysis

In a conventional optical fiber, the value of the normalized frequency V determines the number of waveguide modes, given by [34]:

$$V = \frac{2\pi r}{\lambda}\sqrt{\left(n_{co}^2 - n_{cl}^2\right)} \tag{3}$$

with n_{co} is the effective core index, n_{cl} is the effective cladding index, $k = 2\pi / \lambda$ is the wave number and r is the core radius. The effective refractive index is strongly dependent on wavelength and is an important parameter for improving fiber nonlinearity, providing great flexibility in the design of PCFs.

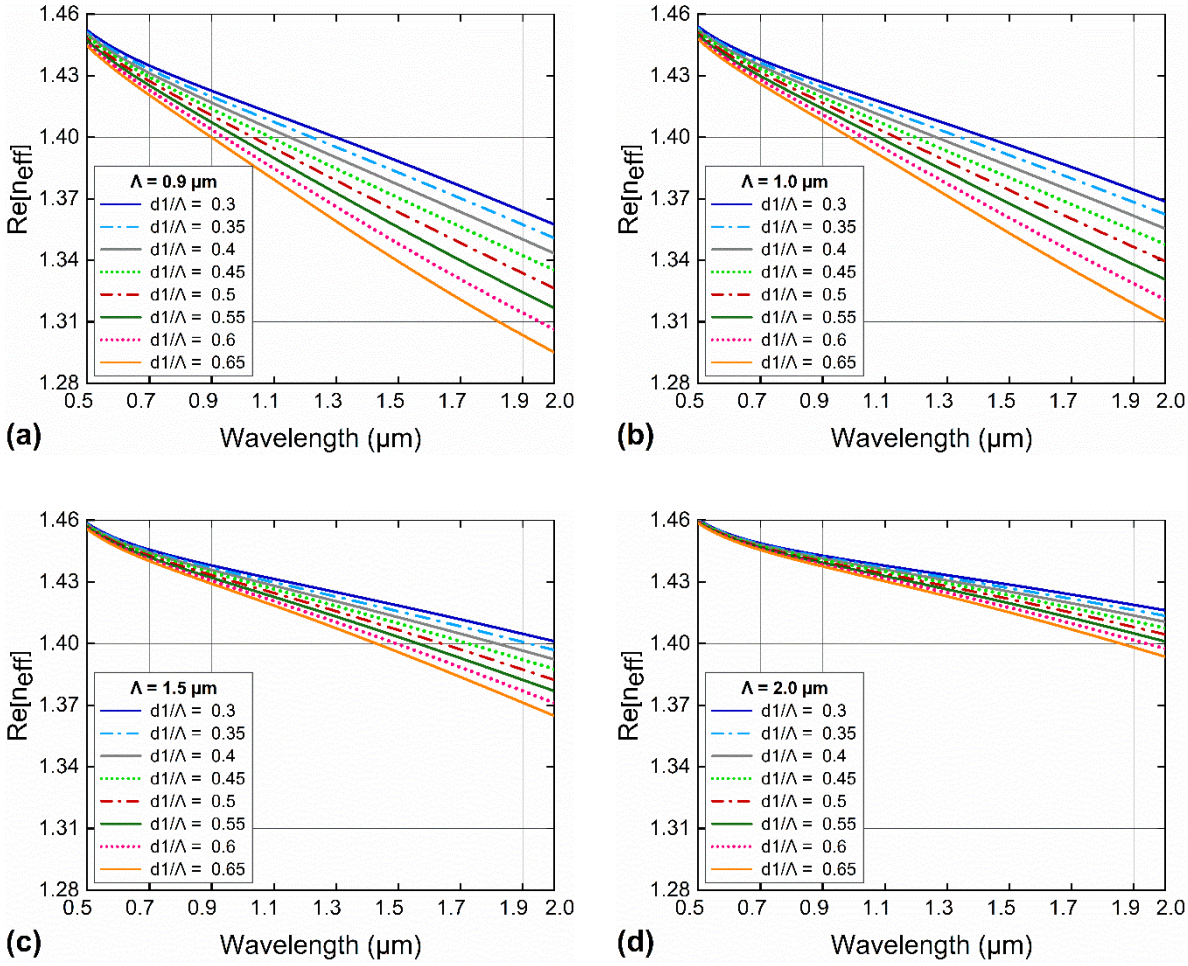

Figure 2. The effective refractive index's real part variation as a function of wavelength with different values of d_1/Λ and Λ = 0.9 μm, 1.0 μm, 1.5 μm, and 2.0 μm.

In order to calculate the effective refractive index, the LPCF is assumed to be a step-index fiber with a wavelength-dependent cladding index. So, the effective refractive index for different LPCF structures can be evaluated by the FDE method. The variations of effective refractive index as a function of wavelength are plotted in Fig. 2. The effective index will lower down as the wavelength increases. This is because the field avoiding the air holes at short wavelengths results in a cladding index close to the refractive index of silica at short wavelengths while the field intensity inside the air holes can be significant at long wavelengths, making only significantly lower refractive index. For each fixed value of Λ, the real part of the effective refractive index decreases with the increase of the diameter of the air holes in the first ring. But it increases with Λ when d_1/Λ is constant. Fibers with large core sizes often face the problem that light modes easily leak from the core to the shell or between the air holes in the rings. The difference of the real effective refractive index of the LPCFs is not too large, the maximum value of n is 1.427 with Λ = 2.0 μm and d_1/Λ = 0.3 and the smallest value is 1.335 when Λ = 0.9 μm and d_1/Λ = 0.65 (Table 1).

Table 1. The real part of the effective refractive index with different values of d_1/Λ and Λ at 1.55 μm wavelength

d_1/Λ	Λ = 0.9 μm	Λ = 1.0 μm	Λ = 1.5 μm	Λ = 2.0 μm
0.3	1.385	1.393	1.417	1.427
0.35	1.38	1.388	1.414	1.426
0.4	1.374	1.383	1.411	1.424
0.45	1.367	1.377	1.408	1.422
0.5	1.36	1.371	1.404	1.42
0.55	1.352	1.364	1.401	1.418
0.6	1.344	1.357	1.397	1.416
0.65	1.335	1.349	1.393	1.413

As light propagates in an optical fiber, different frequency components propagate at different velocities, which are characterized by dispersion properties. The two main components of chromatic dispersion (D) are material dispersion (D_M) and waveguide dispersion (D_W) according to the following formula (4, 5) [34]. Chromatic dispersion is a function of wavelength λ, the speed of light in a vacuum c, and the real part of the effective index $Re[n_{eff}]$ of the guided mode.

$$D(\lambda) = D_M + D_W \tag{4}$$

$$D(\lambda) = -\frac{\lambda}{c}\frac{d^2\,\mathrm{Re}\left[n_{\mathrm{eff}}\right]}{d\lambda^2} \tag{5}$$

The diverse dispersion properties with anomalous and all-normal dispersion are easily observed in Fig. 3, which depicts the dependence of dispersion on the wavelength of LPCFs. In the case of Λ = 0.9 μm, the dispersion curves gradually lower, closer to the zero-dispersion line in the wavelength region of about 0.9 μm to 2.0 μm as d_1/Λ increases. There are three anomalous dispersion curves with one ZDW, corresponding to d_1/Λ equal to 0.3−0.4. As d_1/Λ increases further, the dispersion curves shift below the horizontal axis, becoming all-normal dispersion, except for d_1/Λ = 0.65. Among them, only the dispersion curve corresponding to d_1/Λ = 0.4 has a ZDW close to the wavelength of 1.55 μm (which is the pumping wavelength of commercial lasers). Furthermore, the LPCF with d_1/Λ = 0.45 has very flat and low value dispersion properties. This implies that a clever adjustment of the structural parameters (e.g. increasing Λ) will make this dispersion curve flatter, closer to zero dispersion. Indeed, when Λ = 1.0 μm, the dispersion curve with d_1/Λ = 0.45 becomes an ultra-flattened all-normal dispersion curve with a low value of ±0.44 ps/nm.km covering the wavelength region of 530 nm. In addition, the

d_1/Λ = 0.55, 0.6 structures no longer exhibit all-normal dispersion but become anomalous dispersion with two ZDWs. For LPCFs with larger cores (Λ = 1.0 µm, 1.5 µm) whose dispersion is anomalous properties with one or two ZDWs. SC studies based on soliton dynamics would be suitable for these LPCFs. However, the ZDWs shift towards shorter wavelengths with increasing d_1/Λ (Table 2). The selection of pump wavelengths when using these LPCFs in the SC process is very important, satisfying two conditions: first, the wavelength at the local maximum points of the dispersion curve will give low ZDW values; second, the pump wavelength of commercial lasers is 1.55 µm.

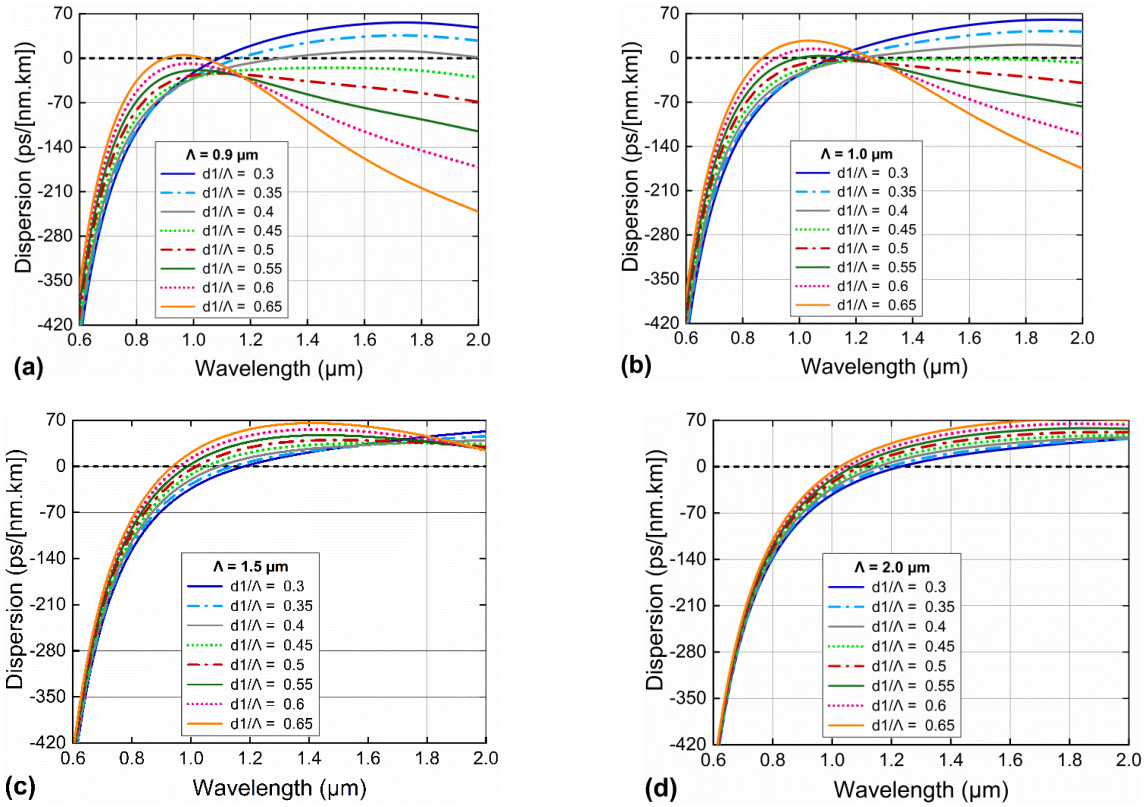

Figure 3. The chromatic dispersion characteristics as a function of wavelength with different values of d1/Λ and Λ = 0.9 µm, 1.0 µm, 1.5 µm, and 2.0 µm.

Table 2. The ZDW's value of LPCFs with various d_1/Λ and Λ = 0.9 µm, 1.0 µm, 1.5 µm, and 2.0 µm

d_1/Λ	Λ = 0.9 µm		Λ = 1.0 µm		Λ = 1.5 µm	Λ = 2.0 µm
	ZDW_1	ZDW_2	ZDW_1	ZDW_2	ZDW_1	ZDW_1
0.3	1.09		1.116		1.179	1.227
0.35	1.157		1.157		1.139	1.19
0.4	1.306		1.215		1.093	1.152
0.45	D < 0		D < 0		1.051	1.123
0.5	D < 0		D < 0		1.017	1.094
0.55	D < 0		0.997	1.173	0.986	1.071
0.6	D < 0		0.916	1.224	0.96	1.047
0.65	0.897	1.04	0.869	1.253	0.936	1.025

Table 3 compares the flatness and fluctuations of dispersion in the wide wavelength region of LPCF (Λ = 1.0 µm, d_1/Λ = 0.45) with previous publications. Most of the ultra-flattened near-zero dispersion was achieved in the design of silica- or composite-based solid-core PCFs (such as ZBLAN) by modifying the sizes of the air holes in the rings so that they are different which can lead to complexities in fabricating fibers. Very few works claim to find such dispersions in fibers with liquid-infiltrated cores. Table 3 also demonstrates that the LPCF with carbon tetrachloride in this study has a lower dispersion value and is flatter in a broader wavelength range.

Table 3. Comparison of the flatness and fluctuations of dispersion of LPCF (Λ = 1.0 µm, d_1/Λ = 0.45) with ultra-flattened chromatic dispersion in previous publications

Materials	D (ps/nm.km)	Ultra-flattened dispersion bandwidth (nm)	Refs.
LPCF with carbon tetrachloride	±0.44	530	This work
Silica-PCF	±0.66	400	[35]
ZBLAN-PCF	±1.05	300	[36]
LPCF with ethanol	±1.04	500	[37]
LPCF with toluene	±0.947	500	[2]
Silica-PCF3	±3.345	420	[38]
Silica-PCF4	±4.304	492	[38]
LPCF with ethanol	±5.0	about 500	[39]
ZBLAN-PCF	±1.1	600	[40]
PCF with selective liquid	± 0.41	452	[41]

The spectral expansion and spectral characterization during SC generation are strongly governed by nonlinear effects related to soliton or non-soliton dynamics. Generally, there are two important features of dispersion that are of interest to many SC generation research groups: all-normal dispersion and anomalous dispersion with one or more ZDWs. The low-noise, flat-top SC spectrum is the result of the fiber being pumped at a wavelength corresponding to the normal dispersion regime. In contrast, in order to have a broader SC spectrum, but more difficult to control noise, the optical fiber is excited in an anomalous dispersion profile, and the pump wavelength is often chosen close to the point corresponding to the local maximum value of the dispersion curve. Based on the above preliminary results, we suggest three LPCFs with suitable structure and dispersion for detailed analysis of other nonlinear properties. The first fiber called #F_1 with Λ = 0.9 µm, d_1/Λ = 0.4 has anomalous dispersion with ZDW = 1.306 µm. Nonlinear effects with soliton dynamics such as SF, SSFS, stimulated Raman scattering, etc. will be the main mechanisms for spectral expansion if this fiber is used for SC generation with a pump wavelength of 1.33 µm greater than ZDW. The second fiber is #F_2 with Λ = 1.0 µm, d_1/Λ = 0.55, the anomalous dispersion of this fiber has two ZDWs, including ZDW_1 = 0.997 µm and ZDW_2 = 1.173 µm, the recommended pumping wavelength is 1.064 µm. With two ZDWs close together, FWM can be phase matched and it becomes the main cause for the spectral expansion while soliton dynamics are arrested and play an almost negligible role in the formation of the supercontinuum [42]. The third fiber #F_3 (Λ = 1.0 µm, d_1/Λ = 0.45) which possesses ultra-flattened near-zero dispersion, with a recommended pumping wavelength at 1.55 µm in an all-normal dispersion regime, is expected to produce a very broad, smooth, flat-top SC spectrum, and less noise [2] under the influence of SPM, OWB, FWM. The dispersion values at the pump wavelengths of the three fibers are 1.405 ps/nm.km, 3.328 ps/nm.km, and −1.938 ps/nm.km, respectively (Fig. 4a). These values are very small, which will help the SC spectrum to be expanded more when using these LPCFs for supercontinuum generation.

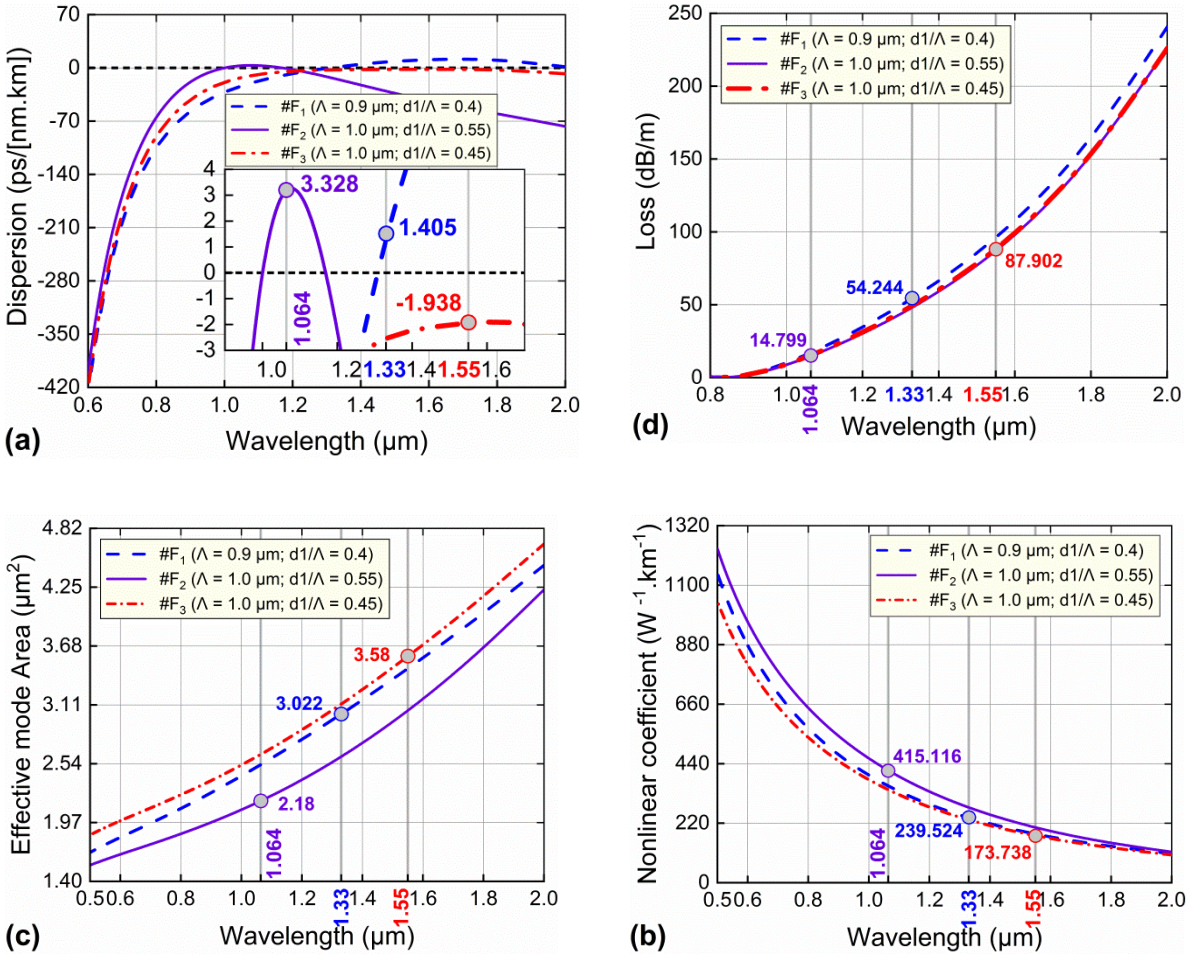

Figure 4. The dispersion and nonlinear properties of the three suggested fibers.

The nonlinear coefficient is inversely proportional to the effective mode area A_{eff}, quantified for the strength of the nonlinear interaction, calculated via the nonlinear refractive index for material n_2 and wavelength λ, as follows [43]:

$$\gamma(\lambda) = 2\pi \frac{n_2}{\lambda A_{\text{eff}}} \tag{6}$$

The effective mode area is an important fiber parameter because it relates the total mode power to the average field intensity inside the nonlinear region and is employed to study the optimal parameters of optical fibers. A_{eff} is determined by the amplitude of the transverse electric field (E) propagating inside the optical fiber [43].

$$A_{\text{eff}} = \frac{\left(\int_{-\infty}^{\infty} \int_{-\infty}^{\infty} |E|^2 \, dxdy \right)^2}{\int_{-\infty}^{\infty} \int_{-\infty}^{\infty} |E|^4 \, dxdy} \tag{7}$$

The confinement loss characterizes depends on the wavelength and the imaginary part of the effective refractive index, which is characterized by the gradual decrease in power with propagation distance as light propagates in an optical fiber, is defined by the following formula [43].

$$L_c = 8.686 \frac{2\pi}{\lambda} \mathrm{Im}[n_{\mathrm{eff}}(\lambda)] \quad (8)$$

Figure 4 presents the dispersion and nonlinear properties of the three suggested fibers. The structural parameters and the values at the pump wavelengths of the characteristic quantities are also-calculated and displayed in Table 4. The nonlinear coefficient decreases with increasing wavelength as shown in Fig. 4b. The leakage of modes of low frequency waves from the core into the cladding, or between the air holes of different rings is responsible for the decrease in the nonlinear coefficient (or increase in the effective mode area) in this wavelength region. The core size is also an important factor in determining the degree of light confinement in the core, because of the smallest core size (Table 4), #F_2 fiber has the highest nonlinear coefficient in the survey wavelength range. This means that the effective mode area of this fiber has the smallest value, since the two coefficients are inversely proportional to each other. At the pump wavelengths, the values of the nonlinear coefficients of the three fibers are 239.524 $W^{-1}.km^{-1}$, 415.116 $W^{-1}.km^{-1}$, and 173.738 $W^{-1}.km^{-1}$, respectively, corresponding to the effective mode area value of 3.022 μm^2, 2.18 μm^2, 3.58 μm^2. The nonlinear coefficient has a great influence on the choice of input power of SC processes. The input power will be low if the LPCFs have a high nonlinear coefficient, like a few hundred $W^{-1}.km^{-1}$. Meanwhile, the low effective mode area value at long wavelengths will help to broaden the spectrum towards the blue and red wavelengths of the SC spectral region. We obtained unexpected confinement loss values of 54.244 dB/m, 14.799 dB/m, 87.902 dB/m at the pump wavelengths 1.33 μm, 1.064 μm, 1.55 μm, respectively. Although the L_c value of a few tens of dB/m is not very high compared to previous reports, we hope that it does not affect the SC quality much.

Table 4. The structural parameters and the values at the pump wavelengths of the characteristic quantities of three suggested fibers

#	D_c (μm)	Λ (μm)	d_1/Λ	Pump wavelength (μm)	$Re[n_{\mathrm{eff}}]$ (real)	A_{eff} (μm^2)	γ ($W^{-1}.km^{-1}$)	D (ps/nm.km)	L_c (dB/m)
#F_1	1.37	0.9	0.40	1.33	1.388	3.022	239.524	1.405	54.244
#F_2	1.34	1.0	0.55	1.064	1.401	2.18	415.116	3.328	14.799
#F_3	1.46	1.0	0.45	1.55	1.377	3.58	173.738	−1.938	87.902

Table 5 verifies the value of characteristic quantities at different pumping wavelengths of the three proposed fibers compared with several previous publications on LPCFs with hollow cores filled with different liquids. Although the nonlinear coefficients of the three fibers are proposed to be lower than that of the chloroform, toluene-infiltrated LPCF [4, 5], we achieve a lower dispersion value and a flatter dispersion. Furthermore, compared with the published reports listed in Table 5, the values of the effective mode area of the three fibers in this paper are smaller, which has important implications for the SC spectrum expansion towards the long wavelength region despite the higher confinement loss. It can be seen that the simultaneous optimization of dispersion and nonlinear properties of LPCFs is very difficult, this depends a lot on the idea of designing and modifying the structures of LPCFs accordingly.

Table 5. The values of proposed three-fiber characteristic quantities at pump wavelength in comparison with previous works

#	Pump wavelength (μm)	A_{eff} (μm^2)	γ (W^{-1}.km^{-1})	D (ps/nm.km)	L_c / attenuation (dB/m)
#F_1	1.33	3.022	239.524	1.405	54.244
#F_2	1.064	2.18	415.116	3.328	14.799
#F_3	1.55	3.58	173.738	−1.938	87.902
#F_1 [5], chloroform	1.03	1.5	1290	−24	–
#F_2 [5], chloroform	1.03	4.48	440	7.6	–
#I_0.3 [4], toluene	1.55	7.79	2132.575	−7.784	40
#I_0.35 [4], toluene	1.55	78.9	2890.276	−1.19	120
#F_1[16], tetrachloroethylene	1.88	433.2	156.9	−15.0	4.0
#F_2[16], tetrachloroethylene	1.88	16.67	40.79	3.20	4.2
#F_3[16], tetrachloroethylene	1.88	359.1	189.3	−4.85	5.3
#F_1 [18], carbon tetrachloride	1.35	–	–	12.0	–
#F_2 [18], carbon tetrachloride	1.55	10.58	–	−4.37	–
#F_1 [18], carbon tetrachloride	1.55	11.83	–	–	–
#F_1 [18], carbon tetrachloride	1.4	–	–	–	1.58
#F_2 [18], carbon tetrachloride	1.4	–	–	–	1.85

4. Conclusion

By cleverly modifying the structural parameters of the LPCFs with carbon tetrachloride, we effectively controlled the dispersion property and achieved near-zero ultra-flattened dispersion with the value of ±0.44 ps/ nm.km in 530 nm wavelength region. The difference in the radii of air holes as well as the distance between the core and the holes can also cause complexity in fiber fabrication, although such fibers can still be fabricated experimentally. The diversity in dispersion properties including anomalous and all-normal dispersion has helped us to propose three fibers with reasonable structure and dispersion value for detailed analysis of nonlinear properties. The first fiber (Λ = 0.9 μm, d_1/Λ = 0.40) is expected to emit SC with soliton dynamics because of the 1.33 μm pump wavelength in the anomalous dispersion mode and the small dispersion value of 1,405 ps/nm.km. The SC spectrum will be broadened by the FWM effect when pumped at 1,064 μm where the soliton dynamics can be suppressed because the second fiber (Λ = 1.0 μm, d_1/Λ = 0.55) has anomalous dispersion consisting of two very close ZDWs. With a small all-normal dispersion value and a flatness spread over a wide wavelength region, we expect the third fiber (Λ = 1.0 μm, d_1/Λ = 0.45) to emit a very broad SC spectrum with non-soliton dynamics including SPM followed by OWB. Besides, the proposed three fibers have a high nonlinear coefficient, a small effective mode area, and suitable confinement loss for SC generation application. In experimentally, carbon tetrachloride-infiltrated PCFs are more favorable to broadband SC all-fiber sources due to the low attenuation of carbon tetrachloride. Therefore, the propagation length can be lower than that of toluene-filled fibers. However, the problems associated with the fusion splicing of liquid core PCFs and standard silica fibers need to be systematically investigated before they can become

truly useful in applications. Although so far there have been published about various modifications of the fusion splicing method up to now.

Acknowledgment

This research is funded by University of Education, Hue University under grant number NCM. T.23–02.

References

[1] T. N. Thi, D. H. Trong, B. T. L. Tran, T. D. Van, L. C. Van, Optimization of Optical Properties of Toluene-Core Photonic Crystal Fibers with Circle Lattice for Supercontinuum Generation, Journal of Optics, Vol. 51, 2022, pp. 678-688, https://doi.org/10.1007/s12596-021-00802-y.

[2] T. N. Thi, D. H. Trong, L. C. Van, Supercontinuum Generation in Ultra-Flattened Near-zero Dispersion PCF with C_7H_8 Infiltration, Optical and Quantum Electronics, Vol. 55, 2023, pp. 93, https://doi.org/10.1007/s11082-022-04351-x.

[3] V. T. Hoang, R. Kasztelanic, A. Anuszkiewicz, G. Stepniewski, A. Filipkowski, S. Ertman, D. Pysz, T. Wolinski, K. D. Xuan, M. Klimczak, R. Buczynski, All-Normal Dispersion Supercontinuum Generation in Photonic Crystal Fibers with Large Hollow Cores Infiltrated with Toluene, Optical Materials Express, Vol. 8, No. 11, 2018, pp. 3568-3582, https://doi.org/10.1364/OME.8.003568.

[4] L. C. Van, A. Anuszkiewicz, A. Ramaniuk, R. Kasztelanic, K. D. Xuan, V. C. Long, M. Trippenbach, R. Buczyński, Supercontinuum Generation in Photonic Crystal Fibres with Core Filled with Toluene, Journal of Optics, Vol. 19, No. 12, 2017, pp. 125604, https://doi.org/10.1088/2040-8986/aa96bc.

[5] L. C. Van, V. T. Hoang, V. Cao Long, K. Borzycki, K. D. Xuan, V. T. Quoc, M. Trippenbach, R. Buczyński, J. Pniewski, Optimization of Optical Properties of Photonic Crystal Fibers Infiltrated with Chloroform for Supercontinuum Generation, Laser Physics, Vol. 29, No. 7, 2019, pp. 075107–9, https://doi.org/10.1088/1555-6611/ab2115.

[6] H. Zhang, S. Chang, J. Yuan, D. Huang, Supercontinuum Generation in Chloroform-Filled Photonic Crystal Fibers, Optik, Vol. 121, No. 9, 2010, pp. 783-787, https://doi.org/10.1016/j.ijleo.2008.09.026.

[7] C. C. Wang, W. M. Li, N. Li, W. Q. Wang, Numerical Simulation of Coherent Visible-To-Near-Infrared Supercontinuum Generation in the $CHCl_3$-Filled Photonic Crystal Fiber with 1.06 μm Pump Pulses, Optics & Laser Technology, Vol. 88, 2017, pp. 215-221, https://doi.org/10.1016/j.optlastec.2016.09.020.

[8] L. C. Van, V. T. Hoang, V. C. Long, K. Borzycki, K. D. Xuan, V. T. Quoc, M. Trippenbach, R. Buczyński, J. Pniewski, Supercontinuum Generation in Benzene-Filled Hollow-Core Fibers, Optical Engineering, Vol. 60, No. 11, 2021, pp. 116109, http://doi.org/10.1117/1.OE.60.11.116109.

[9] L. C. Van, B. T. L. Tran, T. N. Thi, D. H. Trong, T. D. Van, T. D. Mai, H. T. Ngoc, T. T. Doan, K. D. Quoc, Comparison of Supercontinuum Generation Spectral Intensity in Benzene-Core PCFs with Diferent Types of Lattices in the Claddings, Optical and Quantum Electronics, Vol. 54, 2022, pp. 840, https://doi.org/10.1007/s11082-022-04218-1.

[10] L. C. Van, V. T. Hoang, V. C. Long, K. Borzycki, K. D. Xuan, V. T. Quoc, M. Trippenbach, R. Buczyński, J. Pniewski, Supercontinuum Generation in Photonic Crystal Fibers Infiltrated with Nitrobenzene, Laser Physics, Vol. 30, No. 3, 2020, pp. 035105, https://doi.org/10.1088/1555-6611/ab6f09.

[11] R. Zhang, J. Teipel, H. Giessen, Theoretical Design of A Liquid-Core Photonic Crystal Fiber for Supercontinuum Generation, Optics Express, Vol. 14, Iss. 15, 2006, pp. 6800-6812, https://doi.org/10.1364/OE.14.006800.

[12] L. C. Van, T. N. Thi, D. H. Trong, B. T. L. Tran, N. V. T. Minh, T. D. Van, T. L. Canh, Q. H. Dinh, K. D. Quoc, Comparison of Supercontinuum Spectrum Generating by Hollow Core PCFs Filled with Nitrobenzene with Different Lattice Types, Optical and Quantum Electronics, Vol. 54, 2022, pp. 300, https://doi.org/10.1007/s11082-022-03667-y.

[13] J. Wen, B. Liang, W. Qin, W. Sun, C. He, K. Xiong, High Coherent Supercontinuum Generation in Nitrobenzene Liquid-Core Photonic Crystal Fiber with Elliptical Air-Hole Inner Ring, Optical and Quantum Electronics, Vol. 54, 2022, pp. 817, https://doi.org/10.1007/s11082-022-04234-1.

[14] Y. Guo, J. Yuan, K. Wang, H. Wang, Y. Cheng, X. Zhou, B. Yan, X. Sang, C. Yu, Generation of Supercontinuum and Frequency Comb in a Nitrobenzene-Core Photonic Crystal Fiber with All-Normal Dispersion Profile, Optics Communications, Vol. 481, 2021, pp. 126555, https://doi.org/10.1016/j.optcom.2020.126555.

[15] L. C. Van, B. T. L. Tran, T. D. Van, N. V. T. Minh, T. N. Thi, H. P. N. Thi, M. H. T. Nguyen, V. T. Hoang, Supercontinuum Generation in Highly Birefringent Fiber Infiltrated with Carbon Disulfide, Optical Fiber Technology, Vol. 75, 2023, pp. 103151, https://doi.org/10.1016/j.yofte.2022.103151.

[16] H. V. Le, V. T. Hoang, H. T. Nguyen, V. C. Long, R. Buczynski, R. Kasztelanic, Supercontinuum Generation in Photonic Crystal Fibers Infiltrated with Tetrachloroethylene, Optical and Quantum Electronics, Vol. 53, 2021, pp. 187, https://doi.org/10.1007/s11082-021-02820-3.

[17] J. M. Dudley, G. Genty, S. Coen, Supercontinuum Generation in Photonic Crystal Fiber, Reviews of Modern Physics, Vol. 78, No. 4, 2006, pp. 1135-1184, https://doi.org/10.1103/RevModPhys.78.1135.

[18] Q. H. Dinh, J. Pniewski, H. L. Van, A. Ramaniuk, V. C. Long, K. Borzycki, K. D. Xuan, M. Klimczak, R. Buczyński, Optimization of Optical Properties of Photonic Crystal Fibers Infiltrated with Carbon Tetrachloride for Supercontinuum Generation with Subnanojoule Femtosecond Pulses, Applied Optics, Vol. 57, No. 14, 2018, pp. 3738-3746, https://doi.org/10.1364/AO.57.003738.

[19] T. N. Thi, D. H. Trong, B. T. L. Tran, L. C. Van, Flat-Top and Broadband Supercontinuum Generation in CCl_4-Filled Circular Photonic Crystal Fiber, Journal of Nonlinear Optical Physics & Materials, 2022, https://doi.org/10.1142/S021886352350042X.

[20] T. N. Thi, D. H. Trong, L. C. Van, Comparison of Supercontinuum Spectral Widths in CCl_4-Core PCF with Square and Circular Lattices in the Claddings, Laser Physics, Vol. 33, No. 5, 2023, pp. 055102–13, https://doi.org/10.1088/1555-6611/acc240.

[21] H. V. Le, V. T. Hoang, G. Stępniewski, T. L. Canh, N. V. T. Minh, R. Kasztelanic, M. Klimczak, J. Pniewski, K. X. Dinh, A. M. Heidt, R. Buczyński, Low Pump Power Coherent Supercontinuum Generation in Heavy Metal Oxide Solid-Core Photonic Crystal Fibers Infiltrated with Carbon Tetrachloride Covering 930–2500 nm, Optics Express, Vol. 29, No. 24, 2021, pp. 39586-39600, https://doi.org/10.1364/OE.443666.

[22] V. T. Hoang, R. Kasztelanic, A. Filipkowski, G. Stępniewski, D. Pysz, M. Klimczak, S. Ertman, V. C. Long, T. R. Woliński, M. Trippenbach, K. D. Xuan., M. Śmietana, R. Buczyński, Supercontinuum Generation in an All-Normal Dispersion Large Core Photonic Crystal Fiber Infiltrated with Carbon Tetrachloride. Optical Materials Express, Vol. 9, No, 5, 2019, pp. 2264-2278, https://doi.org/10.1364/OME.9.002264.

[23] V. T. Hoang, R. Kasztelanic, G. Stępniewski, K. D. Xuan, V. C. Long, M. Trippenbach, M. Klimczak, R. Buczyński, J. Pniewski, Femtosecond Supercontinuum Generation Around 1560 nm in Hollow-Core Photonic Crystal Fibers Filled with Carbon Tetrachloride, Applied Optics, Vol. 59, No. 12, 2020, pp. 3720-3725, https://doi.org/10.1364/AO.385003.

[24] B. T. L. Tran, L. C. Van, A New Type of Supercontinuum Generation in Hexagonal Lattice C_6H_6-Core PCF with Broadband and Low-Power Pump, International Journal of Modern Physics B, 2023, https://doi.org/10.1142/S0217979224503533.

[25] J. Challenor, Toxicology of Solvents, Rapra Technology Ltd, United Kingdom, 2002, ISBN: 1-85957-296-0, https://doi/10.1093/occmed/52.6.363-a.

[26] M. Vieweg, S. Pricking, T. Gissibl, Y. Kartashov, L. Torner, H. Giessen, Tunable Ultrafast Nonlinear Optofluidiccoupler, Optics Letters, Vol. 37, No. 6, 2012, pp. 1058-1060, https://doi.org/10.1364/OL.37.001058.

[27] J. Meister, R. Franzen, G. Eyrich, J. Bongartz, N. Gutknecht, P. Hering, First Clinical Application of A Liquid-Corelight Guide Connected to an Er: YAG Laser for Oral Treatment of Leukoplakia, Laser in Medical Science, Vol. 25, No. 5, 2010, pp. 669–673, https://doi.org/10.1007/s10103-010-0782-0.

[28] C. Z. Tan, Determination of Refractive Index of Silica Glass for Infrared Wavelengths by IR Spectroscopy, Journal of Non-Crystalline Solids, Vol. 223, No. (1-2), 1998, pp. 158-163, https://doi.org/10.1016/s0022-3093(97)00438-9.

[29] K. Moutzouris, M. Papamichael, S. C. Betsis, I. Stavrakas, G. Hloupis, D. Triantis, Refractive, Dispersive and Thermo-Optic Properties of Twelve Organic Solvents in the Visible and Near-Infrared, Applied Physics B, Vol. 116, No. 3, 2013, pp. 617-622, https://doi.org/10.1007/s00340-013-5744-3.

[30] K. Saitoh, N. J. Florous, M. Koshiba, Theoretical Realization of Holey Fiber with Flat Chromatic Dispersion and Large Mode Area: An Intriguing Defected Approach, Optics Letters, Vol. 31, No. 1, 2006, pp. 26-28, https://doi.org/10.1364/OL.31.000026.

[31] G. Stępniewski, J. Pniewski, D. Pysz, J. Cimek, R. Stępień, M. Klimczak, R. Buczyński, Development of Dispersion-Optimized Photonic Crystal Fibers Based on Heavy Metal Oxide Glasses for Broadband Infrared Supercontinuum Generation with Fiber Lasers, Sensors, Vol. 18, No. 12, 2018, pp. 4127, https://doi.org/10.3390/s18124127.

[32] Z. Zhu, T. G. Brown, Full-Vectorial Finite-Difference Analysis of Microstructured Optical Fibers, Optical Materials Express, Vol. 10, No. 7, 2002, pp. 853-864, https://doi.org/10.1364/OE.10.000853.

[33] S. Kedenburg, M. Vieweg, T. Gissibl, H. Giessen, Linear Refractive Index and Absorption Measurements of Nonlinear Optical Liquids in The Visible and Near-Infrared Spectral Region, Optical Materials. Express, Vol. 2, No. 11, 2012, pp.1588-1611, https://doi.org/10.1364/OME.2.001588.

[34] R. K. Sinha, A. D. Varshney, Dispersion Properties of Photonic Crystal Fiber: Comparison by Scalar and Fully Vectorial Effective Index Methods, Optical and Quantum Electronics, Vol. 37, No. 8, pp. 711-722, 2005, https://doi.org/10.1007/s11082-005-3196-7.

[35] A. Medjouri, L. M. Simohamed, O. Ziane, A. Boudrioua, Z. Becer, Design of a Circular Photonic Crystal Fiber with Flattened Chromatic Dispersion using a Defected Core and Selectively Reduced Air Holes: Application to Supercontinuum Generation at 1.55 μm, Photonics and Nanostructures - Fundamentals and Applications, Vol. 16, 2015, pp. 43-50, https://doi.org/10.1016/j.photonics.2015.08.004.

[36] A. Medjouri, E. B. Meraghni, H. Hathroubi, D. Abed, L. M. Simohamed, O. Ziane, Design of ZBLAN Photonic Crystal Fiber with Nearly Zero Ultra-Flattened Chromatic Dispersion for Supercontinuum Generation, Optik, Vol. 135, 2017, pp. 417-425, https://doi.org/10.1016/j.ijleo.2017.01.082.

[37] H. V. Le, V. L. Cao, H. T. Nguyen, A. M. Nguyen, R. Buczyński, R. Kasztelanic, Application of Ethanol Infiltration for Ultra-Flattened Normal Dispersion in Fused Silica Photonic Crystal Fibers, Laser Physics, Vol. 28, 2018, pp. 115106, https://doi.org/10.1088/1555-6611/aad93a.

[38] Y. Huang, H. Yang, S. Zhao, Y. Mao, S. Chen, Design of Photonic Crystal Fibers with Flat Dispersion and Three Zero Dispersion Wavelengths for Coherent Supercontinuum Generation in Both Normal and Anomalous Regions, Results in Physics, Vol. 23, 2021, pp. 104033, https://doi.org/10.1016/j.rinp.2021.104033.

[39] P. Kumar, K. F. Fiaboe, J. S. Roy, Design of Nonlinear Photonic Crystal Fibers with Ultra-Flattened Zero Dispersion for Supercontinuum Generation, ETRI Journal, Vol. 42, No. 2, 2020, pp. 282-291, https://doi.org/10.4218/etrij.2019-0024.

[40] T. Huang, Q. Wei, Z. Wu, X. Wu, P. Huang, Z. Cheng, P. P. Shum, Ultra-Flattened Normal Dispersion Fiber for Supercontinuum and Dissipative Soliton Resonance Generation at 2 μm, IEEE Photonics Journal, Vol. 11, No. 3, 2019, pp. 7101511, https://doi.org/10.1109/JPHOT.2019.2915265.

[41] P. S. Maji, P. R. Chaudhuri, Supercontinuum Generation in Ultra-Flat Near Zero Dispersion PCF with Selective Liquid Infiltration, Optik, Vol. 125, No. 20, 2014, pp. 5986-5992, https://doi.org/10.1016/j.ijleo.2014.07.026.

[42] A. Ghanbari, A. Kashaninia, A. Sadr, H. Saghaei, Supercontinuum Generation for Optical Coherence Tomography using Magnesium Fluoride Photonic Crystal Fiber, Vol. 140, 2017, pp. 545-554, https://doi.org/10.1016/j.ijleo.2017.04.099.

[43] G. P. Agrawal, Nonlinear Fiber Optics (5th Edition), Elsevier, Amsterdam, ISBN: 978-0-12-397023-7, 2013, https://doi.org/10.1016/C2011-0-00045-5.